AIAA Propulsion and Energy Forum
August 24-28, 2020, VIRTUAL EVENT
AIAA Propulsion and Energy 2020 Forum

10.2514/6.2020-3724

Evaluation of the influence of radiation on a GH_2/GO_2 rocket combustor

Bo Li[1] Wei Yao[2] and Xuejun Fan[3]
Key Laboratory of High-Temperature Gas Dynamics, Institute of Mechanics, CAS, Beijing

100190, China

School of Engineering Science, University of Chinese Academy of Science, Beijing 100049, China

When the temperature exceeds 3000 K, the radiation effect may become non-ignorable. It is easy to reach such high temperatures for liquid propellant rocket engines fuelled by hydrogen-oxygen. However, the role of thermal radiation has been rarely studied for hydrogen-oxygen rocket combustor. In this study, the effect of radiation on a GH_2/GO_2 rocket combustor was investigated by using Discrete Ordinates model (DO), Improved Delayed Detached Eddy Simulation (IDDES) and a Dynamic Zone Flamelet combustion Model (DZFM). Through incorporating radiation, the wall heat flux was better reproduced compared with those without radiation. The flow fields were further analyzed to reveal the influence of radiation on the flow structures.

Nomenclature

p	=	pressure, Pa
T	=	temperature, K
ρ	=	density, kg.m^{-3}
u	=	velocity, m/s
R_u	=	universal gas constant
ν_t	=	eddy viscosity
τ_{ij}	=	viscous stress tensor
i	=	time index during navigation
j	=	waypoint index
Pr_t	=	turbulent Prandtl number
Sc_t	=	turbulent Schmidt number
$\tilde{Y}_k$	=	mass fraction of species k
$\bar{\omega}_k$	=	averaged mass production rate of species k
DO	=	Discrete Ordinates model
LES	=	Large-eddy modelings
IDDES	=	Improved Delayed Detached Eddy Modeling
CMC	=	Conditional Moment Closure
DZFM	=	Dynamic Zone Flamelet Model

I. Introduction

LIQUID propellant rocket engines are widely used and play a critical role in aerospace[1]. Hydrogen is a common fuel for liquid rocket engines for its high specific energy on a mass basis and can be safely transported in pipelines[2]. A thorough understanding of mixing and reaction of GH_2/GO_2 and GH_2/LO_2 injected combustor at high temperatures and velocities is critical for the design of supersonic combustors and the liquid rocket propulsion system[3]. However, the experimental investigations of supersonic combustion remain limited, which not only

[1] PHD student, Institute of Mechanics (CAS), libo2@imech.ac.cn.
[2]Associate Professor, Institute of Mechanics (CAS), weiyao@imech.ac.cn, AIAA member (Corresponding author).
[3] Professor, Institute of Mechanics (CAS), xfan@imech.ac.cn, AIAA lifetime member (Corresponding author).

because the cost to set such an experimental rig is often prohibitively high for most researchers, but also for the limitation of measurement technology under the extremely high pressure and temperature operating conditions. While, with the development of computer technology, computational fluid dynamics (CFD) method can be applied to predict the combustion behaviors for a detailed evaluation of the combustion system. Numerical analysis to evaluate the effects of different numerical models, .e.g., those for turbulence, combustion, and thermal radiation, is critical to provide guidelines for the optimal numerical configurations[4].

Up to now, numerous modelings on supersonic hydrogen-oxygen combustion in rocket combustor has been conducted. Oefelein and Yang[5] performed pioneering modeling of supercritical mixing and combustion of two-dimensional (2-D) GH_2/LO_2 within LES/laminar-chemistry framework. Furthermore, in Oefelein's later study[6], the model was extended to investigate the three-dimensional (3-D) flow evolution and flame structure in a shear coaxial unit-element model rocket. For a relatively quick computational turnaround, Menon et al.[7] performed axisymmetric modeling of LO_2/GH_2 combustion using a simple eddy breakup model. However, the prediction of heat flux is not wholly satisfactory. Later, Menon et al.[8] use the laminar chemistry model conducted a 3-D LES of supercritical GO_2/GH_2 combustion in a single-element GH_2/GO_2 shear coaxial injector, the prediction of the wall heat flux captured the trend of measured data fairly well. Recently, Huo and Yang[3] conducted the modeling of GH_2/GO_2 combustion under supercritical conditions using different combinations of turbulence closure and combustion models. When special attention was given to the prediction of wall heat flux, the LES/flamelet combination shows the best results. The numerical results were also compared with other studies[3, 6, 8, 9], which performed with different turbulence and combustion models. A detailed comparison for the advantages and challenges of turbulence-combustion models for aero-propulsion applications have been published in the review of Gonzalez-Juez[10] and Miller[11].

Earlier works have shown that thermal radiation will affect the heat transfer process and combustion characteristics for most combustion systems. Silva et al.[5] performed numerical modeling of the non-premixed combustion of natural gas in atmospheric air to study the radiation effect, which indicates that thermal radiation strongly affects the temperature field and heat transfer but has negligible effect on the chemical reaction rates. Morvan et al.[12] conducted modeling of methane-air radiating turbulent diffusion flame using high order finite volume method, and the results confirmed that 20-25% of the combustion heat release is radiated away from the flame. Ilbas[13] has done systematic modeling of turbulent non-premixed hydrogen and hydrogen–hydrocarbon flame and found the results with the radiation models are in better agreement with the measurements compared with the results without radiation model. All the above studies are based on hydrocarbon fuel combustions. Burrows[14] conducted a pioneering experiment of radiation for the combustion of liquid-oxygen jets in gaseous hydrogen, and some essential combustion characteristics have been concluded. Cirrone et al.[15] modeled the thermal radiation in cryogenic hydrogen jet fires by Discrete Ordinates (DO) model[16], and confirmed that the radiation strongly affects the flow fields. The researches about thermal radiation are very limited for the modeling of rocket combustors, especially in the modeling of supersonic combustion. However, when the temperature above 3000 K, which can be easily arrived for liquid propellant rocket engines fuelled by hydrogen-oxygen, the radiation effect may not be simply neglected. Therefore, it is necessary to evaluate the effect of radiation on the wall heat transfer and combustion characteristics in the modeling of rocket combustors.

This study aims to evaluate the effect of radiation on a GH_2/GO_2 rocket combustor by numerical methods. The modeled heat transfer and combustion characteristics with and without radiation will be compared. Section II describes the numerical methods, including the physical model, meshing, boundary conditions, as well as models for turbulence, combustion, and radiation. Section III compares the predictions of wall heat flux and fow fields with the measurement and those in the literature. Finally, the main conclusion is drawn in Section IV.

II. Numerical Methods

A. Physical model description, boundary conditions, and meshing

In the current study, the experiment of the supercritical GH_2/GO_2 combustion with a single shear-coaxial injector was conducted by Marshall et al.[17]. Fig. 1 gives the schematic diagram of the rocket combustor, (a) the overall size of the combustor, (b) the size of its coaxial injector. As can be seen in Fig. 1(a), there is a 0.43mm recess for oxygen injector, the cylinder combustion chamber within a size of 38.1 mm and 337 mm in diameter and length respectively, and the throat diameter of the exit nozzle is 8.17 mm. Fig. 1 (b) gives the major sizes of the coaxial injector, where the oxygen is injected from the inner annular center with an outer diameter of 6.3 mm, and the hydrogen fuel is injected from the outer annular with a diameter of 7.49 mm.

According to the experimental setup, all the wall temperature is fixed, and the rail wall temperature distribution of the combustion chamber uses the value of experimental measured as shown in Fig.1 (a), the bottom of the combustion

chamber and the nozzle section are assumed to be fixed at 755 K, and the nozzle temperature is assumed to be fixed at 510 K. The other boundary conditions are set according to the experimental parameters of the supersonic combustion listed in Table. 1. It can be seen that both the stream of fuel and oxidant are injected as the same static pressure of 5.2 MPa with the static temperature of 711 K and 800 K respectively. The reference pressure for the current calculations is also set at 5.2 MPa. The Mach numbers of oxidant and fuel streams are 0.31 and 0.51, corresponding to the speeds of 150 m/s and 750 m/s. No-slip conditions are used for all wall surfaces. Supersonic boundary conditions are applied to the nozzle exit.

Here, the hexahedral, block-unstructured grid with the axisymmetric pattern was employed to mesh the whole computational, where the external injector tube is excluded. Regions in the jet core, the jet shear layers, and the near-wall zone are refined specifically, as shown in Fig. 2. Finally, the total grid size of the computational domain is 15.23 million.

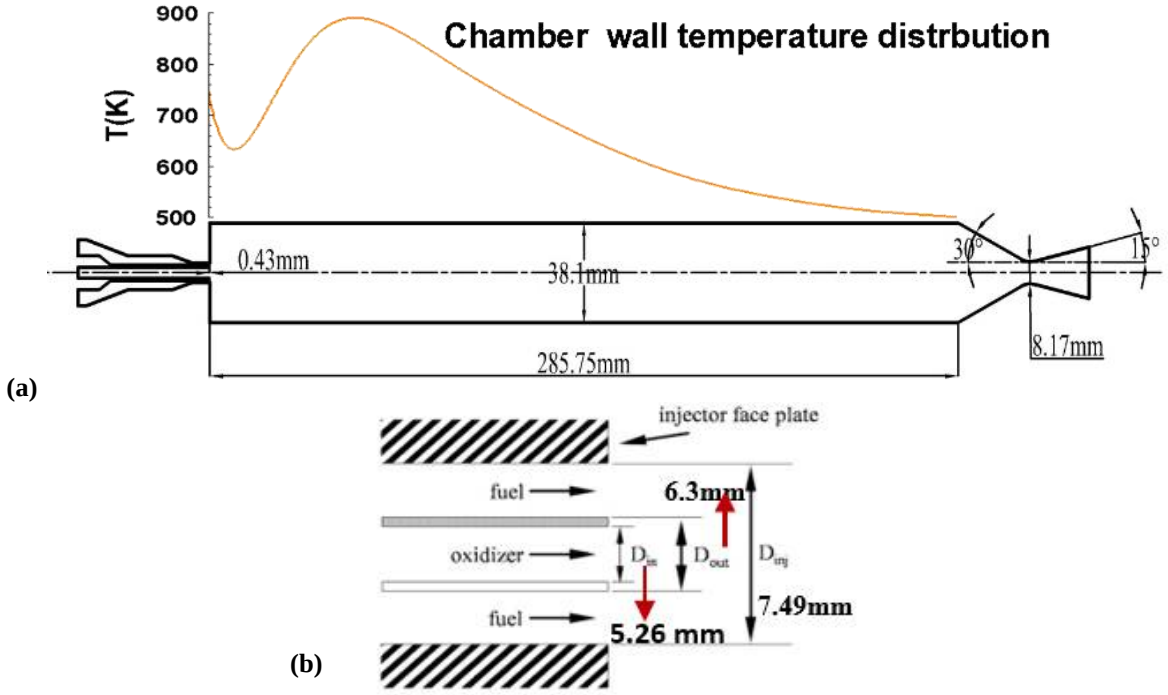

Fig. 1. Schematic diagram of the rocket combustor, (a) the general size of the combustor, (b) the size of its coaxial injector.

Table 1 Experimental boundary condition

	Hydrogen	Oxygen
Mach number	0.31	0.51
velocity	150 m/s	750 m/s
static temperature	711 K	800 K
static pressure	5.2 MPa	5.2 MPa
composition		
Y_{H_2}	40.2%	0
Y_{O_2}	0	94.5%
Y_{H_2O}	59.8%	5.5%

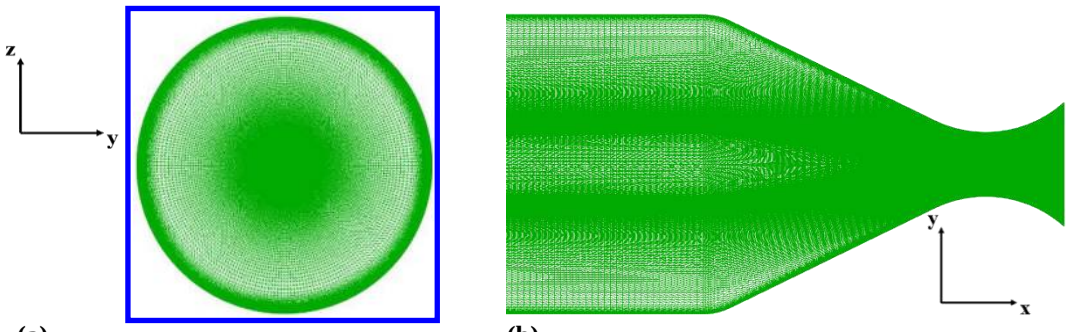

(a) (b)

Fig. 2. The mesh details on the (a) jet orifice at z=0 and (b) the bottom near the nozzle exit.

B. Governing equations

In this study, the unsteady and three-dimensional Favre-averaged compressible Navier-Stokes (N-S) equations of mass, momentum, energy, and species concentration are written in the following form:

$$\frac{\partial \bar{\rho}}{\partial t}+\frac{\partial \bar{\rho}\tilde{u}_j}{\partial x_j}=0 \tag{1}$$

$$\frac{\partial \bar{\rho}\tilde{u}_i}{\partial t}+\frac{\partial \bar{\rho}\tilde{u}_j\tilde{u}_i}{\partial x_j}+\frac{\partial \bar{p}}{\partial x_i}-\frac{\partial \tilde{\tau}_{ij}}{\partial x_j}=-\frac{\partial \tau_{ij}}{\partial x_j} \tag{2}$$

$$\frac{\partial \bar{\rho}\tilde{H}_t}{\partial t}+\frac{\partial \bar{\rho}\tilde{u}_j\tilde{H}_t}{\partial x_j}-\frac{\partial}{\partial x_j}\left(\bar{\rho}D_T\frac{\partial \tilde{H}_t}{\partial x_j}+\sum_{k=1}^{L}\bar{\rho}D_k\frac{\partial \tilde{Y}_k}{\partial x_j}\tilde{H}_k\right)-\frac{\partial \bar{p}}{\partial t}-\frac{\partial \tilde{u}_j\tilde{\tau}_{ij}}{\partial x_j}=-\frac{\partial \Psi_{T,j}}{\partial x_j} \tag{3}$$

$$\frac{\partial \bar{\rho}\tilde{Y}_k}{\partial t}+\frac{\partial \bar{\rho}\tilde{u}_j\tilde{Y}_k}{\partial x_j}-\frac{\partial}{\partial x_j}\left(\bar{\rho}D_k\frac{\partial \tilde{Y}_k}{\partial x_j}\right)=-\frac{\partial \Psi_{k,j}}{\partial x_j}+\bar{\omega}_k \tag{4}$$

$$\bar{p}=\bar{\rho}R\tilde{T} \tag{5}$$

where the overbar "-" and the tilde "~" recurrent spatial-filtering variables and Favre-filtering operation respectively, t denotes the time; The variables p , T, ρ, τ_{ij} , u_i is the pressure, temperature, density, viscous stress tensor and the velocity component in x_i direction (spatial dimension i = 1, 2, 3), respectively; $\tilde{H}_t=\tilde{H}+0.5\tilde{u}_i^2$ is the total absolute enthalpy obtained as the sum of the absolute enthalpy $\tilde{H}$ and the resolved kinetic energy; $\tilde{Y}_k$ and $\bar{\omega}_k$ recurrents the mass fraction and the averaged mass production rate of species k (k = 1 , ..., L, with L the total species number), respectively; D_k and D_T denotes the mixture-averaged mass diffusivity and the thermal diffusivity, respectively. For the combustion is considered far from the drastic phase-change region, the ideal gas law is employed to relate the density, temperature, and pressure of the gas, in which $R=R_u/W$ is the gas constant of the mixture and R_u is the universal gas constant, W is the molar weight of the multicomponent mixture and defined by:

$$W=\left(\sum_{k=1}^{L}Y_k/W_k\right)^{-1} \tag{6}$$

The Soret and Dufour effects are neglected in the current study because of its small contribution in Eqs(3)-(4). And according to the Stokes' hypothesis, the computable average momentum diffusive flux for a Newtonian fluid is given by:

$$\tilde{\tau}_{ij}=\bar{\rho}\nu(\tilde{T})\left(2\tilde{S}_{ij}-\frac{2}{3}\delta_{ij}\tilde{S}_{kk}\right) \tag{7}$$

where ν is the kinetic viscosity and $\tilde{S}_{ij}$ is the rate-of-strain tensor of the computable scales, which is defined as:

$$\tilde{S}_{ij}=\frac{1}{2}\left(\frac{\partial \tilde{u}_i}{\partial x_j}+\frac{\partial \tilde{u}_j}{\partial x_i}\right) \tag{8}$$

For the unclosed terms in the *N-S* equations, additional specific modeling is required. By the gradient diffusion assumption, the turbulent enthalpy flux term $\Psi_{T,j}=\bar{\rho}\left(\widetilde{u_jH_t}-\tilde{u}_j\tilde{H}_t\right)$ and the turbulent species diffusion term $\Psi_{k,j}=\bar{\rho}\left(\widetilde{u_jY_k}-\tilde{u}_j\tilde{Y}_k\right)$ is modeled as Eq.(9) and Eq.(10), respectively.

$$\Psi_{T,j}=-2\bar{\rho}\frac{\nu_t}{Pr_t}\frac{\partial \tilde{H}_t}{\partial x_j} \tag{9}$$

$$\Psi_{k,j}=-2\bar{\rho}\frac{\nu_t}{Sc_t}\frac{\partial \tilde{Y}_k}{\partial x_j} \tag{10}$$

where ν_t is the eddy viscosity, Pr_t is the turbulent Prandtl number and Sc_t is the turbulent Schmidt number.

The thermodynamic and transport properties of the mixture, such as the absolute enthalpy and the specific heat of species, are calculated by the chemical kinetics package CHEMKIN-II. The mixture-viscosity and the thermal conductivity of the species is calculated based on a CHEMKIN-format transport database[18], and the thermal and mass diffusivities are estimated by using the unity turbulent Prandtl and Schmidt number.

C. Models for turbulence, combustion, and radiation

In the near-wall region, the grid number for LES of turbulent boundary layer needs to be resolved scale with the Reynolds number (*Re*) as Re^n, where *n* is large than 1.6[3]. Therefore, a formidable task for practical geometries modeled by LES is the computation-cost. To alleviate the computational difficulties while retain the LES accuracy, the turbulence is treated by Improved Delayed Detached Eddy Modeling (IDDES)[19], in which the near-wall region is modeled by RANS, and the outer flow region is resolved with LES, with a smooth transition between the two regions. Spalart-Allmaras model is employed to model the subgrid length scales, which can improve the wall-bounded behavior prediction, against adverse pressure gradients flow in boundary layers, and is efficient and robust for computation[20].

The turbulent combustion model is another important yet time-consuming factor for CFD. For alleviating the huge computational cost, many acceleration strategies such as ISAT (In Situ Adaptive Tabulation)[21, 22], DAC (Dynamic Adaptive Chemistry)[23-26] and Conditional Moment Closure (CMC) have been used to speed up the solving of combustion chemistry. Particularly, the CMC model is conducted by using one conserved scalar of mixture fraction together with some other status variables. However, the zone divisions of the conventional CMC model are fixed at the beginning, which usually can not adapt to the evolution of combustion fields containing large spatial and timing variations[27]. In the current study, a dynamic zone flamelet model (DZFM) extended from CMC is used, which divides the whole computational domain into different zones according to the time-variant mixture fraction fields and use a local flamelet to describe the chemistry status within each zone. Since the zone division is dynamically adapting to the current flow field, a better local statistical homogeneity can be achieved, and the redistribution effect of conditional variances can be significantly alleviated. More details about the DZFM method can be found in our previous study[28, 29]. Burke's detailed hydrogen/oxygen chemical mechanism with 9 species and 19 reversible reaction steps was adopted to describe the combustion chemistry[30, 31].

Discrete Ordinates (DO) model is used to model the radiative heat transfer in this study. The main assumption of the DO is that the radiation leaving the surface element in a certain range of solid angles can be approximated by a single ray. Compared with the other radiation models, DO model has obvious advantages in accuracy and applicability[32]. First, it is a relatively simple and accurate model, and the accuracy of the model can be further increased by increasing the number of rays. Second, it can be applied to a wide range of optical thickness, which make it especially useful in the modeling of complex combustion in combustors[33]. Third, it can solve the temperature-jump problem[32]. DO model neglects the effect of scattering and assumes that all surfaces are diffuse. The current implementation assumes gray radiation, where the absorption coefficients obtained from the weighted-sum-of-gray-gases model (WSGGM)[34] vary with the gas composition and temperature. Solving a problem with a large number of rays is CPU-intensive[33], a compromise pixelation of 4×4 for the discretization in the polar and azimuthal angles is adopted in this study.

D. Solver and numerical details

In the current study, a density-based finite volume compressible solver, Amber (formerly AstroFoam)[35], is employed to conduct the modeling of GH_2/GO_2 combustion in rocket combustor. Amber is extended from the rhoCentralFoam solver[36], which is also a density-based solver and is suitable for high-speed compressible flows. On the basis of rhoCentralFoam solver, Amber has added modules for the calculation of thermophysical properties, multicomponent transport, and chemical reaction[37]. Amber has been successfully validated in many previous studies, which including both combustion and non-reacting flow. The nonlinear inviscid convective fluxes are evaluated by using a second-order semidiscrete central Kurganov–Tadmor scheme[35]. The third-order spatial accuracy in reconstructing primitive convective fluxes at faces is realized by the scale-selective discretization (SSD) scheme[38]. The temporal integration is advanced by the second-order Crank–Nicholson scheme[36].

The modelings are conducted on the national supercomputer center in Tianjin (TH-1) using 140 CPU cores (Intel(R) Xeon(R) CPU E5-2690v4 with the base frequency of 2.60GHz). The time step is limited both by a maximum Courant number of 0.3 and a user-specified maximum time step of 2×10^{-8} s. The flush through time (FTT) defined based on the length of the combustor flow-path length (0.337 m) and the inlet flow speed of the oxidizer stream (150 m/s) is $2.24\times10^{-3}\ s$. For meaningful data sampling and statistics, the data of the mean combustion field are ensured at least 10 FTTs (≈22.4 ms).

III. Results and discussion

A. Wall heat flux

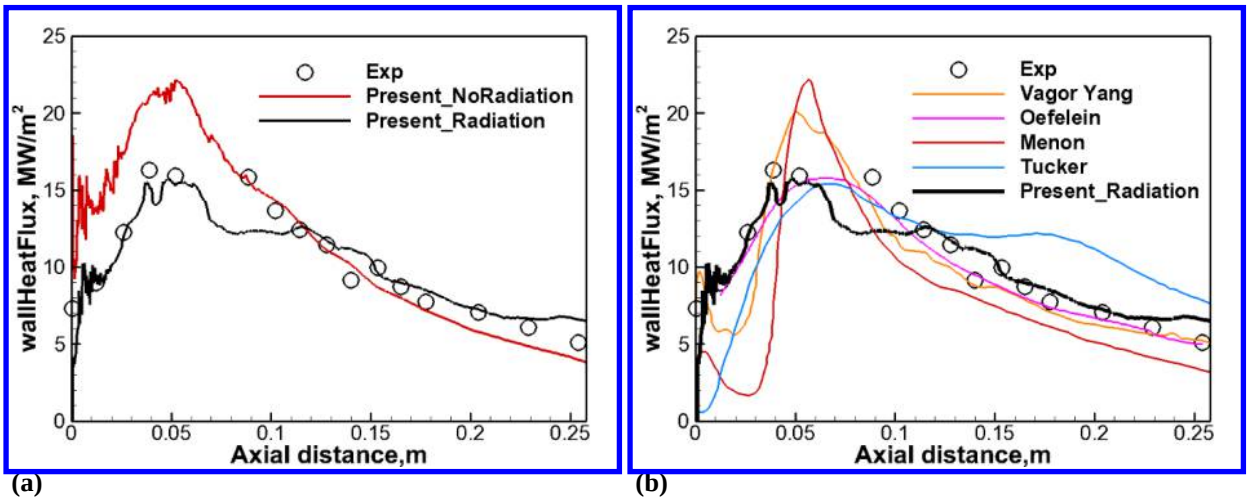

Fig. 3. Wall heat flux distribution (a) with and without radiation, (b) comparison with the predictions in the literature

To verify the performance of the two modelings with and without radiation model, the distributions of the wall heat flux were compared between the measurement and the current modelings, as shown in Fig. 3 (a), in which the symbol denotes the measurement, the black and red solid lines denote the current modeling with and without radiation model, respectively. Both the modelings well predict the heat flux profile in the downstream region. While in the upper region, the modeling ignoring the radiation effect overpredicts the wall heat flux in reference to the experimental measurement, but the one with radiation matches well with only slight underprediction near the peak. To further verify the current modeling work, another comparison was carried out between the predictions in the literature and the current modeling incorporating the radiation effect. As can be seen, the current prediction and Oefelein's prediction provide the best agreements with the experimental data over the entire length of the chamber. Note that Oefelein's modeling has the highest fidelity among all of the others, and the total cell number is 17 times more than this study. This implies that an improvement in the modeling fidelity may help to further improve the agreement. All the other modelings have ignored the radiative heat transfer. The comparison shows that when the gas temperature is as high as nearly 3000 K, the contribution from radiation should be considered.

B. Instantaneous combustion characteristics

Fig. 4 gives the evolution of the vortex structures recurrented by isosurfaces of Q-criterion at the beginning stage of the supersonic GH_2/GO_2 combustion, which is defined as:

$$\Omega = \frac{1}{2}\left(\Omega_{ij}\Omega_{ij} - S_{ij}S_{ij}\right) \tag{8}$$

where S_{ij} and Ω_{ij} denote the strain and rotation tensor, respectively. Here, the isosurfaces are colored by the temperature and set as the value of Q = 5×10^9 s^{-2}. The combustion mainly occurs near the injector exit, where rich vortex structures are formed. The region from x= 0 to x = 0.1 m is refined to better capture the flow evolution.The flush through time (FTT) defined based on the inlet flow speed of the oxidizer stream (150 m/s) is $6.6\times 10^{-4}\ s$. As can be seen, the turbulent transition of the supersonic combustion mainly consist of four flow stages. In Fig.4 (a), under the high injected pressure of 5.2MPa, the shear-coaxial jets burst out of the nozzle, a sizeable symmetric recirculation zone is formed by the jet of H_2 blocked by the quiescent air, and a tip recirculation zone is formed by O_2 with a higher speed of 750 m/s. As time goes on, as shown in Fig. 4(b), the first recirculation zone expands to the downstream due to heat addition by the combustion; meanwhile, the tip recirculation zone shrinks, becomes unstable, and loses symmetry. Then, due to the effect of the shear layer and the Kelvin–Helmholtz (K-H) instabilities, fast mixing results in violent combustion and plenty of finer turbulent structures, shown as Fig. 4 (c). When the time reaches about 1.5 FTT = 1×10^{-3} s, the flow transforms into the fully developed state, as shown in Fig. 4(d). Near the

injector exit, the large-scale Ω shape vortices along the shear layer are rotated by themselves and nesting mutually due to three-dimensional K-H instabilities, while moving in the downstream, where finer structures are broken down from large-scale coherent structures.

Fig. 5 compares the instantaneous snapshots of mass-fraction fields of H_2, O_2, and H_2O with and without radiation. As can be seen in Fig. 5(a), there is an expanding non-reacting core from the injector exit for the high injected pressure. The shear layers in the region of 0-0.03 m are formed due to the large speed difference between the fuel and oxidizer jets. However, the jet core region is larger if incorporating the radiation model. For the radiation case, the duration is about 0.08 m; while for the one without radiation, its duration is smaller than 0.04 m. The radiation causes a similar influence on the core of O_2, as in Fig.5 (b), where the length of O_2 core without radiation is almost three times the radiative one. The breakdown of the jet core is determined by the combined effect of turbulence, reaction, and heat transfer. Due to the radiative heat transfer, the thermal expansion is stronger, which speeds up the breakup of the jet core. The arising large-scale flow structures promote the mixing between the reactants and produce more violent combustion, which can be seen from the richer distribution of H_2O in Fig. 5(c). The more intense heat release also promotes the jet breakup. As expected, the enhanced mixing and combustion reactions near the injector result in lower concentration of H_2O in the downstream.

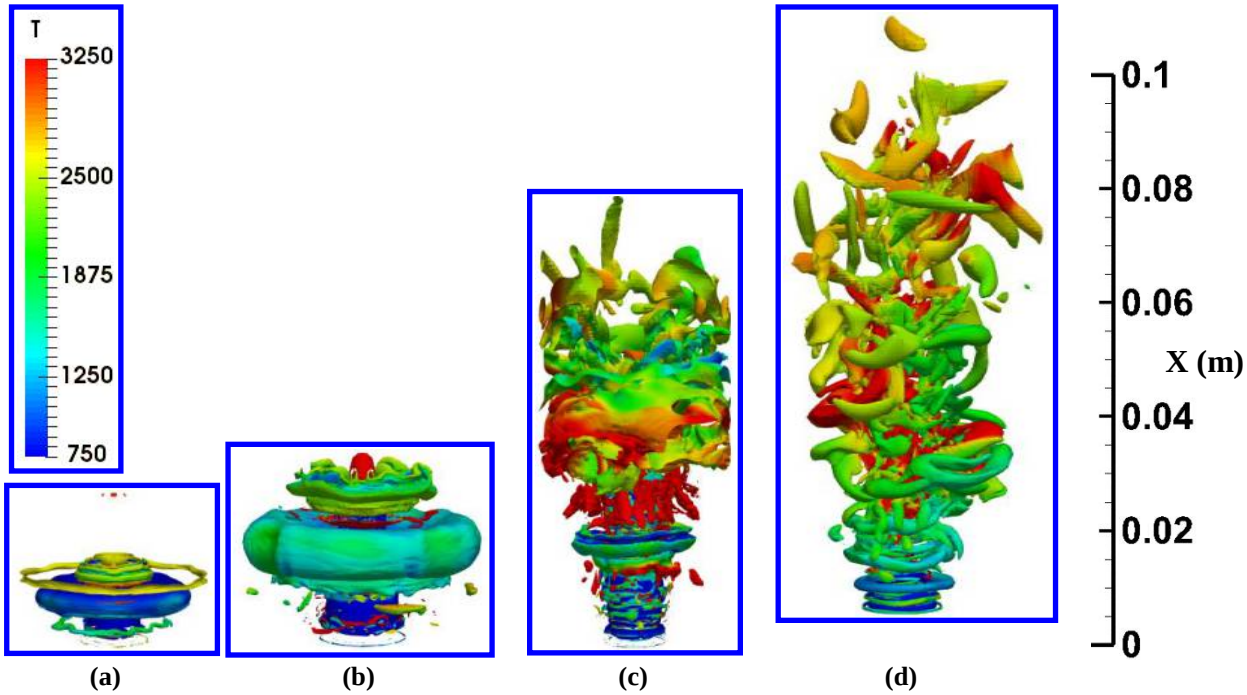

Fig. 4. Development of the 3-D isosurfaces of the Q-criterion ($Q = 5e^9\ s^{-2}$) colored by temperature, (a) t = 1e-5 s, (b) t = 4e-5 s, (c) t = 8e-5 s, and (d) t = 1e-3 s.

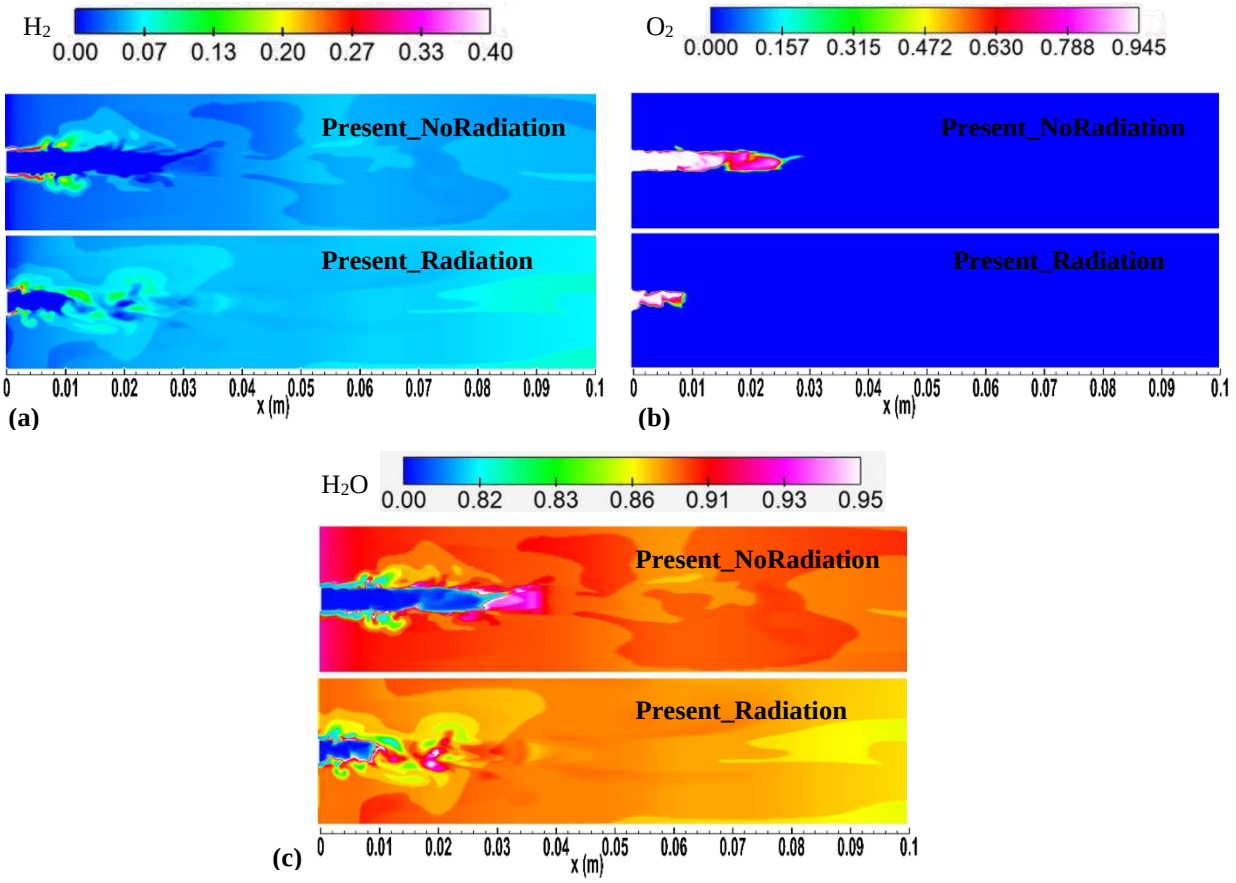

Fig. 5. The comparisons between radiation considered and not for the snapshots of mass-fraction fields of (a) H_2, (b) O_2, and (c) H_2O.

C. Time-averaged combustion characteristics

Fig. 6 compares the time-averaged contour of temperature between the current modelings with and without radiation. Near the injector, a temperature higher than 3500 K is produced. The exit temperature near the nozzle is also around 3000 K. The overall temperature for the modeling with radiation is slightly lower than the radiation-ignored one. However, the temperature in the reacting zone is higher if with radiation, which can be explained by the fact that the influence of the radiation can't be ignored when the temperature is higher than 3000 K.

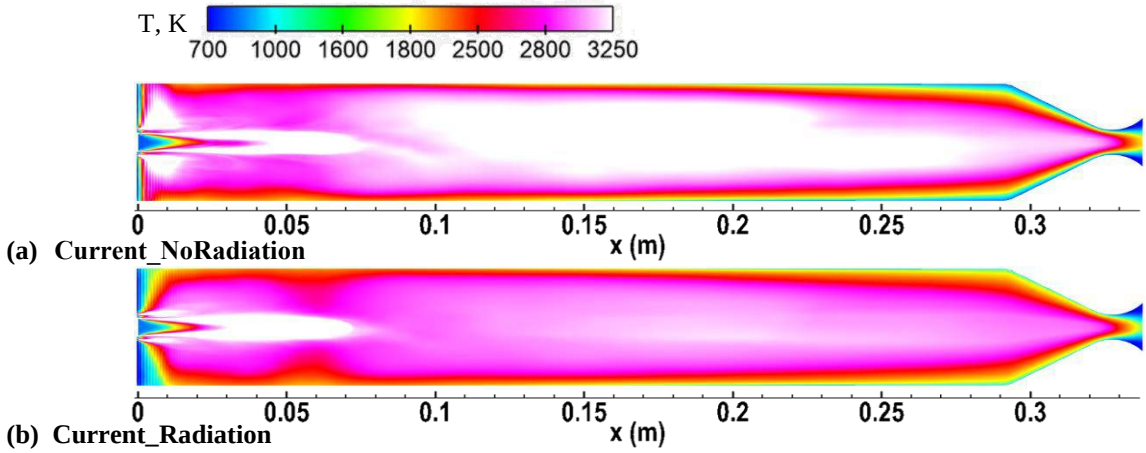

Fig. 6. The comparison of the time-averaged contour of temperature between the current modelings of with and without radiation model.

The time-averaged structure of the recirculation zones is shown in Fig. 7, with superimposed streamlines on the temperature distributions on the interval $0 \leqslant x \leqslant 0.10$ m. The downstream end of the recirculation zone at x = 0.06 m corresponds to the location where the heat flux drops suddenly, implying that the wall heat transfer is significantly influenced by the recirculation. The recirculation zone structure, in terms of size, shape, and location, has a significant impact on the redistribution of species and reaction zones. Therefore, it will significantly affect the wall heat flux on the front chamber part. From the comparison of heat flux profiles, it is found that the modelings conducted by Huo et al. and Oefelein et al. give better agreements with the measurement. Therefore, in the following analysis, only the results of Huo et al. and Oedelein et al. are compared. From Fig. 6, the size, shape, and location of the recirculation zone in each of the four numerical cases are quite different. For the current two modelings, both exhibit a single large recirculation zone, while the one without radiation model is larger but narrower, and centering at a more downstream location. The result of Oefelein is significantly different from the current study. While the result of Huo shows similarity in the shape of a large recirculation zone, but the location and size vary significantly from the current modeling. The similarity can explain why the heat flux predictions by Huo and the current study share similar profiles but different peaks. Both the predictions by Huo and Oefelein show a corner recirculation bubble, but with different sizes.Oefelein's modeling is the only one that exhibits three recirculation zones.

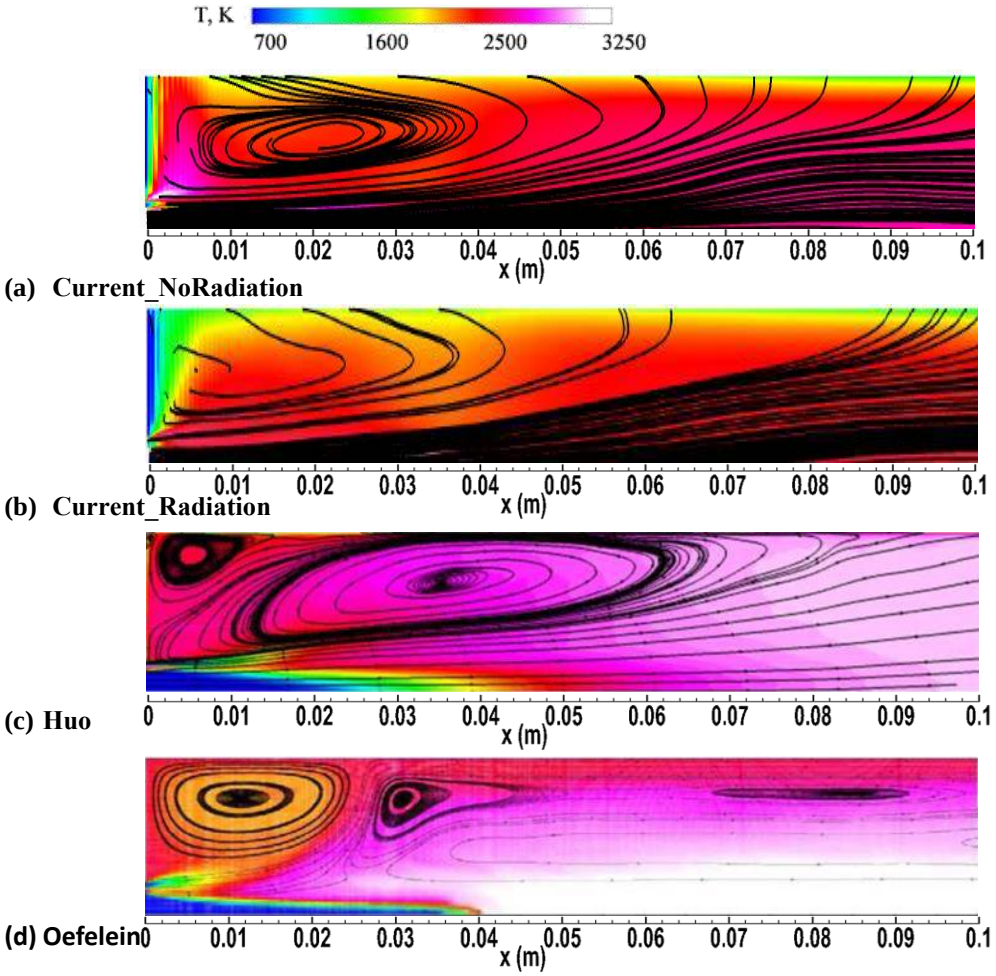

Fig. 7. Comparison of the time-averaged streamlines overlaid on temperature given by (a) the current without radiation model, (b) the current study with the radiation model, (c) Huo et al.[3], and (d) Oefelein[9].

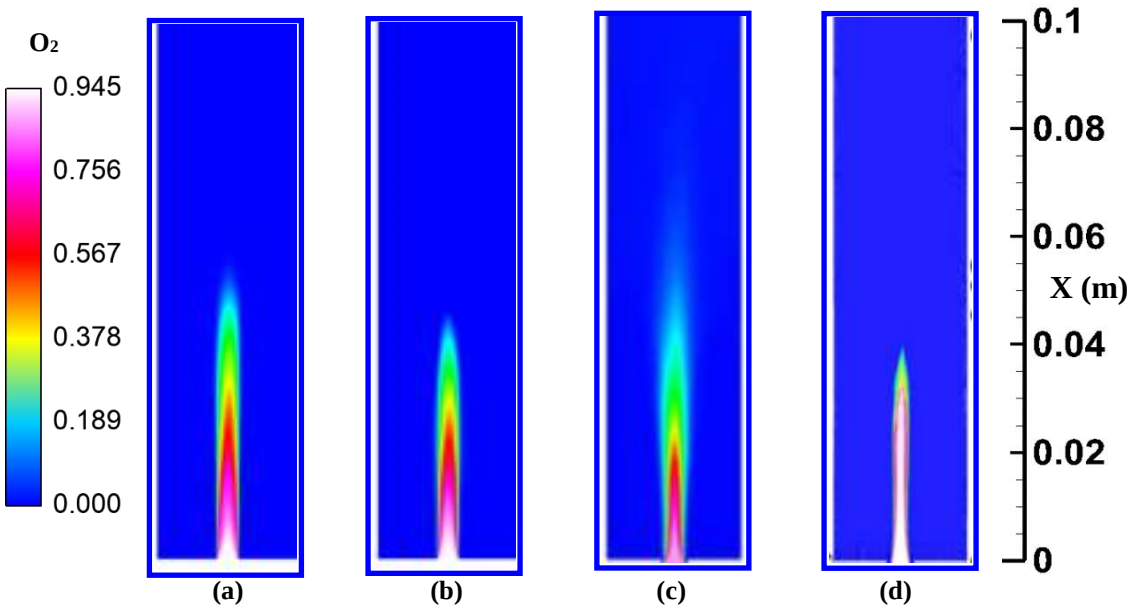

Fig. 8. Time-averaged distributions of oxygen mass fraction given by (a) the current study without radiation model, (b) the current study with the radiation model, (c) Huo et al.[3], and (d) Oefelein[9]

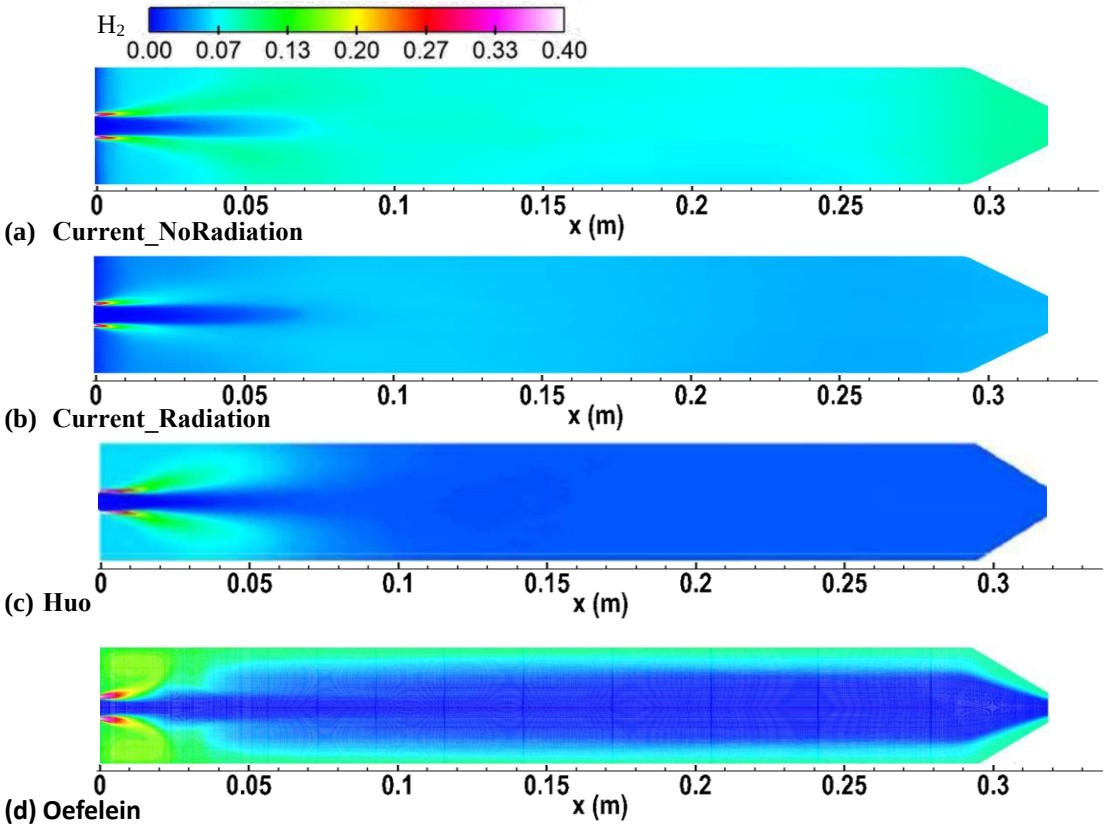

Fig. 9. Time-averaged distributions of hydrogen mass fraction given by (a) the current study without radiation model, (b) the current study with the radiation model, (c) Huo et al.[3], and (d) Oefelein[9].

Figs. 8 and 9 show the distributions of time-averaged oxygen and hydrogen mass fraction in the entire domain. As can be seen, the height of the unburned oxidizer jet and the radial expansion of the hydrogen jet vary from each other. The modeling given by Huo et al. shows the highest height of the unburnt oxidizer jet, while the modeling by Oefelein gives the smallest height for the unburnt oxidizer jet. As in the analysis of the recirculation zone(s), the current modelings exhibit similarity with Huo's modeling for the unburnt oxidizer jet while the latter shows a higher jet core. As expected, the height of unburnt oxidizer jet for the modeling without radiation is larger than the one with radiation. The distributions of H_2 have larger differences, especially for the radial expansion. As can be seen, there is a larger expansion for the modeling with radiation compared with the others. However, the concentration of H_2 for the modeling without radiation is also larger than the other three cases in the middle and upstream regions. In Oefelein's modeling, hydrogen is forced to flow through the gap between the corner bubbles and attach the chamber wall, forming a film of H_2. It is supposed that the film of H_2 provides a thermal barrier, which reduces the wall heat flux to be more coincident with the experiment.

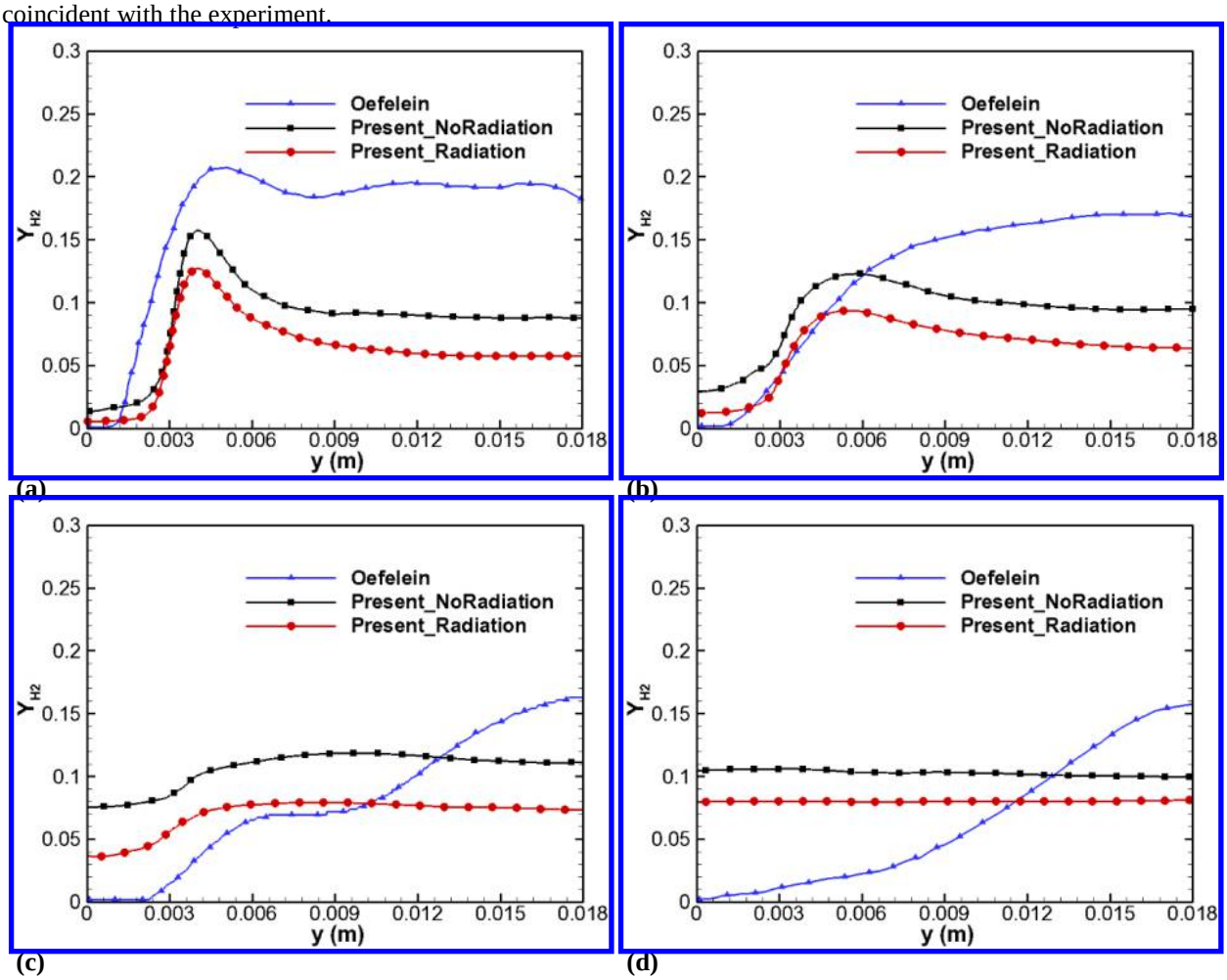

Fig. 10. Comparison of the radial profiles of hydrogen mass fraction at different axial locations, (a) x =0.0125 m, (b) x = 0.025 m, (c) x = 0.05 m, and (d) x = 0.15m.

Fig. 10 compares the radial profiles of hydrogen mass fraction with and without radiation, together with Oefelein's data at the axial locations of 0.0125, 0.025, 0.05, and 0.15 m downstream of the injector. The differences are generally larger between the current predictions and Oefelein's prediction. In the region of $x \leqslant 0.15$ m, the hydrogen mass fraction for the modeling with radiation is smaller than the one without radiation.

IV. Conclusion

This study numerically modeled the mixing and combustion of the single shear-coaxial injector GH_2/GO_2 rocket combustor with and without radiation. The simulational results of the heat transfer and combustion characteristics

were analyzed and compared with the results of the experimental measurement and the data by other researchers. In this study, the mixing in the jet of the coaxial injector was modeled by using Improved Delayed Detached Eddy Modeling (IDDES) based on the background RANS mode of Spalart-Allmaras model, and dynamic zone flamelet model (DZFM) applying local flamelets to different flow regions. Discrete Ordinates model (DO) is used to model the radiative heat transfer in the GH_2/GO_2 rocket combustor, for it is accuracy and wide applicability.

The current prediction with radiation and the Oefelein's prediction show the best agreements with the experimental data over the entire length of the chamber. An improvement in the current modeling fidelity may help to further improve the agreement. The modeling ignoring the radiation effect significantly overpredicts the wall heat flux, which emphasizes that when the gas temperature is as high as nearly 3000 K, the contribution from radiation should be considered. Although radiation is not included in Oefelein's modeling, the wall heat flux is reduced by the thermal barrier effect of the H_2 film formed by the recirculation zones.

Acknowledgments

The research was supported by Training Program of the Major Research Plan of the National Natural Science Foundation of China (Grant No. 91641110), National Key Research and Development Program of China (2019YFB1704200), and the Open founding of National Key Laboratory of Science and Technology on Aero-Engine Aero-Thermodynamics (Grant No. 6142702180307). The authors are also grateful to the National Supercomputer Center in Tianjin for providing the computational resource.

References

[1] Jeff West, D. W., Jeff Lin and Kevin Tucker. "Accuracy Quantification of the Loci-CHEM Code for Chamber Wall Heat Fluxes in a G02_GH2 Single Element Injector Model Problem," *NASA Technical Reports Server*, 2006.

[2] Ó Conaire, M., Curran, H. J., Simmie, J. M., Pitz, W. J., and Westbrook, C. K. "A comprehensive modeling study of hydrogen oxidation," *International Journal of Chemical Kinetics* Vol. 36, No. 11, 2004, pp. 603-622.doi: 10.1002/kin.20036

[3] Huo, H., and Yang, V. "Large-Eddy Simulation of Supercritical Combustion: Model Validation Against Gaseous H2–O2 Injector," *Journal of Propulsion and Power* Vol. 33, No. 5, 2017, pp. 1272-1284.doi: 10.2514/1.b36368

[4] Yılmaz, İ., Taştan, M., İlbaş, M., and Tarhan, C. "Effect of turbulence and radiation models on combustion characteristics in propane–hydrogen diffusion flames," *Energy Conversion and Management* Vol. 72, 2013, pp. 179-186.doi: 10.1016/j.enconman.2012.07.031

[5] Silva, C. V., FranÇA, F. H. R., and Vielmo, H. A. "Analysis of the Turbulent, Non-Premixed Combustion of Natural Gas in a Cylindrical Chamber with and without Thermal Radiation," *Combustion Science and Technology* Vol. 179, No. 8, 2007, pp. 1605-1630.doi: 10.1080/00102200701244710

[6] Oefelein, J. C. "Mixing and Combustion of Cryogenic Oxygen-Hydrogen Shear-Coaxial Jet Flames at Supercritical Pressure," *Combustion Science and Technology* Vol. 178, No. 1-3, 2006, pp. 229-252.doi: 10.1080/00102200500325322

[7] Masquelet, M., Menon, S., Jin, Y., and Friedrich, R. "Simulation of unsteady combustion in a LOX-GH2 fueled rocket engine," *Aerospace Science and Technology* Vol. 13, No. 8, 2009, pp. 466-474.doi: 10.1016/j.ast.2009.07.005

[8] Masquelet, M., and Menon, S. "Large-Eddy Simulation of Flame-Turbulence Interactions in a Shear Coaxial Injector," *Journal of Propulsion and Power* Vol. 26, No. 5, 2011, pp. 924-935.doi: 10.2514/1.48023

[9] Tucker, P. K., Menon, S., Merkle, C. L., Oefelein, J. C., and Yang, V. "Validation of High-Fidelity CFD Simulations for Rocket Injector Design," *44th AIAA/ASME/SAE/ASEE Joint Propulsion Conference & Exhibit*. Vol. AIAA 2008-5226, Hartford, CT, 2008.

[10] Gonzalez-Juez, E. D., Kerstein, A. R., Ranjan, R., and Menon, S. "Advances and challenges in modeling high-speed turbulent combustion in propulsion systems," *Progress in Energy and Combustion Science* Vol. 60, 2017, pp. 26-67.doi: 10.1016/j.pecs.2016.12.003

[11] Miller, R. S., and Foster, J. W. "Survey of Turbulent Combustion Models for Large-Eddy Simulations of Propulsive Flowfields," *AIAA Journal* Vol. 54, No. 10, 2016, pp. 2930-2946.doi: 10.2514/1.j054740

[12] Morvan D, P. B., Loraud JC, Larini M. "Numerical simulation of a methane_air radiating turbulent diffusion flame," *Int J Numer Methods Heat Fluid Flow* Vol. 10, No. 2, 1999, pp. 196-227.

[13] Ilbas, M. "The effect of thermal radiation and radiation models on hydrogen–hydrocarbon combustion modelling," *International Journal of Hydrogen Energy* Vol. 30, No. 10, 2005, pp. 1113-1126.doi: 10.1016/j.ijhydene.2004.10.009

[14] Burrows, M. C. "Radiation Processes Related to Oxygen-Hydrogen Combustion At High Pressures," *NASA Technical Note* Vol. 10, No. 1, 1965, pp. 207-215.doi: 10.1016/S0082-0784(65)80165-5

[15] Cirrone, D. M. C., Makarov, D., and Molkov, V. "Thermal radiation from cryogenic hydrogen jet fires," *International Journal of Hydrogen Energy* Vol. 44, No. 17, 2019, pp. 8874-8885.doi: 10.1016/j.ijhydene.2018.08.107

[16] Siewert, C. E. "A discrete-ordinates solution for radiative-transfer models that include polarization e!ects," *Journal of Quantitative Spectroscopy & Radiative Transfer* Vol. 64, No. 2000, 1998, pp. 227-254.

[17] Marshall, W. M., Pal, S., Woodward, R. D., and Santoro, R. J. "Benchmark wall heat flux data for a GO2/GH2 single element combustor," *41st AIAA/ASME/SAE/ASEE Joint Propulsion Conference*. Vol. AIAA 2005-3572, 2005.

[18] Kee, R. J., Dixon-lewis, G., Warnatz, J., Coltrin, M. E., and Miller, J. A. "A Fortran Computer Code Package For The Evaluation Of Gas-Phase, Multicomponent Transport Properties." Sandia National Laboratories, Livermore, California, 1986.

[19] Shur, M. L., Spalart, P. R., Strelets, M. K., and Travin, A. K. "A hybrid RANS-LES approach with delayed-DES and wall-modelled LES capabilities," *International Journal of Heat and Fluid Flow* Vol. 29, No. 6, 2008, pp. 1638-1649.doi: 10.1016/j.ijheatfluidflow.2008.07.001

[20] Maschninenwesen, F. f. "Detached-Eddy Simulation of a Wall-Mounted Cylinder Flow," *Bachelor's Thesis in Mechanical Engineering*, 2016.

[21] Pope, S. B. "Computationally efficient implementation of combustion chemistry using in situ adaptive tabulation," *Combustion Theory and Modeling* Vol. 1, No. 1, 1997, pp. 41-63.doi: 10.1080/713665229

[22] Yang, B., and Pope, S. B. "Treating chemistry in combustion with detailed mechanisms - In situ adaptive tabulation in principal directions - premixed combustion," *Combustion and Flame* Vol. 112, 1998, pp. 85-112.doi: 10.1016/S0010-2180(97)81759-2

[23] Contino, F., Jeanmart, H., Lucchini, T., and D'Errico, G. "Coupling of in situ adaptive tabulation and dynamic adaptive chemistry: An effective method for solving combustion in engine simulations," *Proceedings of the Combustion Institute* Vol. 33, No. 2, 2011, pp. 3057-3064.doi: 10.1016/j.proci.2010.08.002

[24] Liang, L., Stevens, J. G., and Farrell, J. T. "A dynamic adaptive chemistry scheme for reactive flow computations," *Proceedings of the Combustion Institute* Vol. 32, No. 1, 2009, pp. 527-534.doi: 10.1016/j.proci.2008.05.073

[25] Pepiot-Desjardins, P., and H.Pitsch. "An efficient error-propagation-based reduction method for large chemical kinetic mechanisms," *Combustion and Flame* Vol. 154, 2008, pp. 67-81.doi: 10.1016/j.combustflame.2007.10.020

[26] Lu, T., and Law, C. K. "Linear time reduction of large kinetic mechanisms with directed relation graph: n-Heptane and iso-octane," *Combustion and Flame* Vol. 144, No. 1-2, 2006, pp. 24-36.doi: 10.1016/j.combustflame.2005.02.015

[27] Triantafyllidis, A., Mastorakos, E., and Eggels, R. L. G. M. "Large Eddy Simulations of forced ignition of a non-premixed bluff-body methane flame with Conditional Moment Closure," *Combustion and Flame* Vol. 156, No. 12, 2009, pp. 2328-2345.doi: 10.1016/j.combustflame.2009.05.005

[28] Yao, W., and Fan, X. "Application of dynamic zone flamelet model to a GH2/GO2 rocket combustor," 2019.doi: 10.2514/6.2019-3868

[29] Yao, W. "On the application of dynamic zone flamelet model to large eddy simulation of supersonic hydrogen flame," *Internatinal Journal of Hydrogen Energy*, 2020.doi: 10.1016/j.ijhydene.2020.05.189

[30] Burke, M. P., Chaos, M., Ju, Y., Dryer, F. L., and Klippenstein, S. J. "Comprehensive H2/O2 kinetic model for high-pressure combustion," *International Journal of Chemical Kinetics* Vol. 44, No. 7, 2012, pp. 444-474.doi: 10.1002/kin.20603

[31] Li, J., Zhao, Z., Kazakov, A., and Dryer, F. L. "An Updated Comprehensive Kinetic Model of Hydrogen Combustion," *International Journal of Chemical Kinetics* Vol. 36, No. 10, 2004, pp. 566-575.doi: 10.1002/kin.20026

[32] Siewert, C. E. "The linearized Boltzmann equation_ a concise and accurate solution of the temperature-jump problem," *Journal of Quantitative Spectroscopy & Radiative Transfer* Vol. 77, 2003, pp. 417-432.

[33] Fiala, T., and Sattelmayer, T. "Assessment of existing and new modeling strategies for the simulation of OH* radiation in high-temperature flames," *CEAS Space Journal* Vol. 8, No. 1, 2015, pp. 47-58.doi: 10.1007/s12567-015-0107-z

[34] Smith, T. F., Shen, Z. F., and Friedman, J. N. "Evaluation of coefficients for the weighted sum of gray gases model," *Transactions of the ASME* Vol. 104, 1982, pp. 602-608.

[35] Yao, W., Lu, Y., Wu, K., Wang, J., and Fan, X. "Modeling analysis of an actively-cooled scramjet combustor under different kerosene/air ratios," *Journal of Propulsion and Power* Vol. 34, No. 4, 2018, pp. 975-991.doi: doi.org/10.2514/1.B36866

[36] Weller, H. G., Tabor, G., Jasak, H., and Fureby, C. "A Tensorial Approach to CFD using Object Oriented Techniques," *Computers in Physics* Vol. 12, No. 6, 1997, pp. 620-631.doi: 10.1063/1.168744

[37] Yao, W., Lu, Y., Li, X., Wang, J., and Fan, X. "Improved Delayed Detached Eddy Simulation of a high-Ma regenerative-cooled scramjet combustor based on skeletal kerosene mechanism," 2016.doi: 10.2514/6.2016-4761

[38] Vuorinen, V., Larmi, M., Schlatter, P., Fuchs, L., and Boersma, B. J. "A low-dissipative, scale-selective discretization scheme for the Navier–Stokes equations," *Computers & Fluids* Vol. 70, 2012, pp. 195-205.doi: 10.1016/j.compfluid.2012.09.022